







Universality of charge doping driven metal-insulator transition in Sr_2RhO_4 and role of spin-orbit coupling

Junyoung Kwon ^{1,2,*}, Shoresht Soltani ^{3,4}, Craig Polley,³ Jongkeun Jung,^{1,2} Minsoo Kim ^{1,2}, Donghan Kim ^{1,2}, Jonathan Denlinger,⁵ Dongjoon Song,^{1,†} Yoshiyuki Yoshida,⁶ Wonshik Kyung ^{1,‡} and Changyoung Kim ^{1,2,§}

¹Center for Correlated Electron Systems, Institute for Basic Science, Seoul 08826, Korea

²Department of Physics and Astronomy, Seoul National University, Seoul 08826, Korea

³MAX IV Laboratory, Lund University, SE-22100 Lund, Sweden

⁴Department of Microtechnology and Nanoscience, Chalmers University of Technology, SE-41296 Göteborg, Sweden

⁵Advanced Light Source, Lawrence Berkeley National Laboratory, Berkeley, California 94720, USA

⁶National Institute of Advanced Industrial Science and Technology, Tsukuba 305-8568, Japan



(Received 23 March 2022; revised 9 November 2022; accepted 9 December 2022; published 30 December 2022)

We performed angle-resolved photoemission spectroscopy (ARPES) experiments on an electron-doped Sr_2RhO_4 system $\text{Sr}_{2-x}\text{Ce}_x\text{RhO}_4$ in order to investigate the electron doping-induced metal-insulator transition (MIT). We establish the universality of MIT in electron-doped Sr_2RhO_4 by comparing results from $\text{Sr}_{2-x}\text{La}_x\text{RhO}_4$ and $\text{Sr}_{2-x}\text{Ce}_x\text{RhO}_4$. Via a systematic analysis of doping-dependent transport and ARPES data, we show that the correlation driven MIT with a noninteger electron number in electron-doped Sr_2RhO_4 is universal and thus independent of the dopant. Within the universality, the ARPES analysis shows that the band topology determined by the spin-orbit coupling (SOC) is likely a control parameter of the insulating gap size and critical electron number of the MIT. We present a phase diagram of the insulating phase as a function of the effective SOC and electron number.

DOI: [10.1103/PhysRevB.106.L241114](https://doi.org/10.1103/PhysRevB.106.L241114)

Over the past decade, the concept of a spin-orbit coupling (SOC) driven metal-insulator transition (MIT) has been adopted in the discussion of the electrical and magnetic properties of heavy-element compounds as found in the case of Sr_2IrO_4 [1]. The strong SOC of the Ir in Sr_2IrO_4 leads to $j_{\text{eff}} = 1/2$ pseudospin states that exhibit exotic properties such as Weyl semimetal phases [2,3] or Kitaev quantum spin liquid phases [4,5]. In most of the studies, $5d$ transition metals such as Ir or Os are chosen because of the required strong SOC [1,6]. As a result, the moderate SOC of $4d$ transition metal oxides (TMOs) has been largely ignored; the SOC of $4d$ TMO systems is generally considered insignificant compared with the electron correlation and ligand field. However, recent studies have shown that, even in $4d$ TMOs, SOC can either renormalize band structures [7,8] or induce a Mott state via SOC driven band splitting [9]. The reported role of SOC in the electronic structure suggests possibilities for exotic physical phenomena caused by SOC even in $4d$ TMOs.

A recent study of a novel SOC driven MIT in $\text{Sr}_{2-x}\text{La}_x\text{RhO}_4$ (SL) can be an example. The result from SL suggests that degeneracy lifting of the t_{2g} bands due to SOC can lead to an MIT [10]. It is known from studies of pure

Sr_2RhO_4 that $J_{\text{eff}} = 1/2$ and $3/2$ bands may be formed by a moderate SOC, especially near the Fermi energy [11]. The work on SL showed that full occupation of the $J_{\text{eff}} = 3/2$ band can trigger an MIT in the remaining partially occupied $J_{\text{eff}} = 1/2$ band, without integer filling. The insulating gap of SL provides a unique case in which the gap does not collapse during further charge doping, unlike the ordinary Mott insulators. While angle-resolved photoemission spectroscopy (ARPES) has demonstrated that the band occupation is the primary cause of the MIT, potential issues may arise such as a disorder effect accompanied by the dopant. Thus, further studies are needed to address how the change in SOC affects the gap in the system.

To address these issues, we performed electronic band structure studies of Ce-doped Sr_2RhO_4 via ARPES. The idea is that, if the SOC driven MIT picture is right, one should expect the same MIT in Ce-doped Sr_2RhO_4 with less Ce substitution in comparison to the SL case. Through a comparative study of $\text{Sr}_{2-x}\text{Ce}_x\text{RhO}_4$ (SC) and SL, we find the universality that the MIT occurs in both systems when the SOC driven $J_{\text{eff}} = 3/2$ band is fully occupied. Furthermore, we observe unexpected band renormalization in SC, which is likely due to a change in SOC. We present the quantitative relationship between the SOC strength and insulating gap size, then construct a phase diagram for the MIT.

SC samples were grown using the floating-zone method [10,12]. Off-stoichiometric Rh_2O_3 , SrCO_3 , and CeO_2 powders were mixed and sintered at 1100 °C. The sintered polycrystal was again ground and pressed into a rod, and sintered at 1300 °C. Single-crystal growth proceeded in an image furnace at 20 mm/h growth speed under 10 atm of O_2 . After

*Present address: Department of Physics, Pohang University of Science and Technology, Pohang, Gyeongbuk 37673, Korea.

†Present address: Stewart Blusson Quantum Matter Institute, University of British Columbia, Vancouver, British Columbia V6T 1Z1, Canada.

‡specialtoss@gmail.com

§changyoung@snu.ac.kr

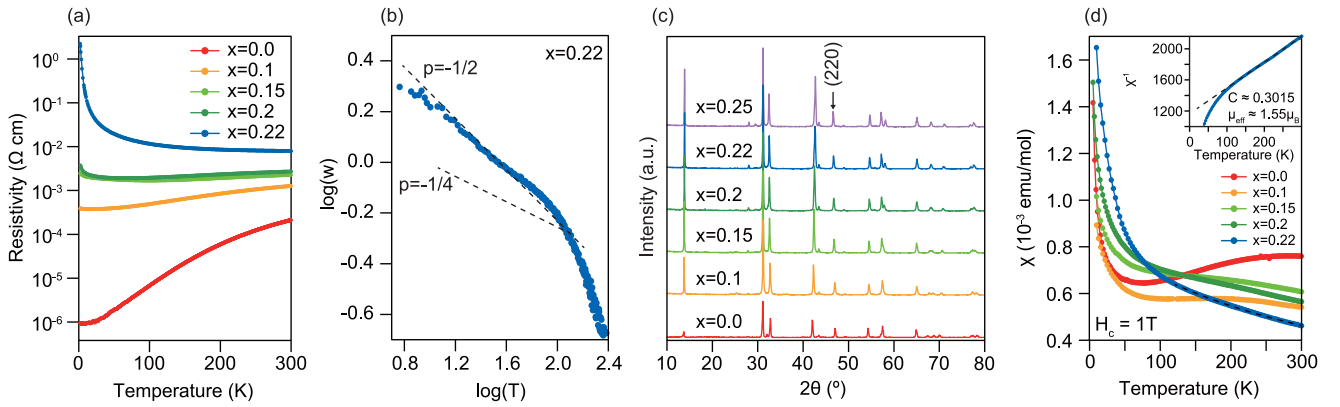


FIG. 1. Physical properties of $\text{Sr}_{2-x}\text{Ce}_x\text{RhO}_4$ (SC). (a) Temperature-dependent in-plane resistivity. (b) Zabrodskii plot [14,15] of the resistivity for $x = 0.22$, where $w = \log(\rho/\rho_0)$. Dashed lines represent Mott ($p = -1/2$) and Efros-Shklovskii ($p = -1/4$) models. The high-temperature part approximately follows $p = -3/2$, which is a non-variable-range hopping behavior, stemming probably from a thermal activation behavior. (c) Doping-dependent x-ray diffraction (XRD) data. The (220) peak is ascribed to the space group of Sr_2RhO_4 ($I4_1/acd$). The inset shows a magnified comparison of the doping-dependent (220) peaks. (d) Doping- and temperature-dependent magnetic susceptibility data. The inset plots the $1/\chi$ of $x = 0.22$. A Curie-type fit (black dashed line) is used to extract the Curie constant C and the effective magnetic moment μ_{eff} .

the growth, the crystals were postannealed under oxygen flow in order to reduce the reported oxygen deficiency [12]. The actual doping level was measured by energy dispersive x-ray spectroscopy as shown in the Supplemental Material (SM) [13]. For the x-ray diffraction (XRD), powder samples were prepared by grinding annealed single crystals. A monochromatized $\text{Cu } K\alpha$ source was used for the measurement. The ARPES measurements were performed at the Bloch beamline of the MAX IV Laboratory, and at the home-laboratory system equipped with a helium discharge lamp (He I light) at Seoul National University. All the measurements were done at 20 K in an ultrahigh vacuum better than 1×10^{-10} Torr.

SC indeed has a doping-dependent MIT as shown in Fig. 1(a). As is the case for the correlation driven MIT in SL [10], the MIT of the SC also occurs around a noninteger value of $x = 0.2$, at which the electron provided by Ce can be at most $0.4e$. However, the noninteger doping rate may indicate that the MIT is a mere consequence of the Anderson localization from the disorder effect. Noting that the MIT of the Anderson localization scenario follows the Mott variable-range hopping (VRH) model, we present in Fig. 1(b) a Zabrodskii plot of the temperature-dependent resistivity for the $x = 0.22$ sample in order to verify whether the Mott VRH model governs the transport. The slope in Fig. 1(b) is the exponent p of the VRH model equation [14,15],

$$\rho = \rho_0 e^{(T/T_0)^p}. \quad (1)$$

At high temperature, thermal excitation of electrons hinders the observation of the VRH resistivity behavior. The slope changes in the low-temperature region, and shows the intrinsic property of the hopping. The low-temperature slope agrees well with the Efros-Shklovskii VRH model ($p = -1/2$) [16] but not with the Mott VRH model ($p = -1/4$) [17], indicating that the insulating $x = 0.22$ sample possesses strongly correlated electronic behavior with a hard energy gap. These results suggest that SC also has a correlation driven MIT with a gap similar to the case of the previously discovered MIT in SL [10].

While the resistivity implies an electronic origin of the MIT, one needs to exclude other factors such as structure change or magnetic ordering. Plotted in Fig. 1(c) are the XRD data for various dopings. The lattice parameters of the undoped system obtained from the XRD data are consistent with the previous results [18,19], and the full width at half maxima (FWHM) of a few selected peaks do not show appreciable doping dependence (please see SM [13]). For the doped compounds, one can consider that the crystal radius of Ce^{4+} (1.16 Å) is smaller than that of Sr^{2+} (1.45 Å) [20]. Therefore, Ce doping accompanies chemical pressure, which may alter the structure from tetragonal to orthorhombic symmetry as Ca^{2+} (1.32 Å) [20] substitution does in Sr_2RuO_4 [21–24]. However, the (220) peak, which should split under a tetragonal to orthorhombic transition [21], does not show any splitting in the doped compounds. Therefore, Ce doping causes only a gradual change in the lattice parameters, not a symmetry change.

The magnetic susceptibility data presented in Fig. 1(d) may also exclude the contribution from the magnetic order. The Pauli-like paramagnetism is identified for $x = 0.0$, as previously reported [19,25]. The Ce doping gradually transforms the system into a Curie-like paramagnetic system. As a result, the $x = 0.22$ agrees well with the Curie behavior ($\chi = C/T$) in the high-temperature regions; the dashed line in the inset is the fitted result. The estimated effective magnetic moment is $\mu_{\text{eff}} = 1.55 \mu_B$. The μ_{eff} is less than the value predicted from $S = 1/2$ ($1.73 \mu_B$), which may be due to the noninteger electron number. The transformation from itinerant Pauli-like to localized Curie-like magnetism may also suggest localization of the electron via the MIT. The above investigations on the structure and magnetism of SC show that the MIT of SC is not from a structural change or magnetic ordering, but should be due to a correlation effect as deduced based on the Efros-Shklovskii VRH behavior in the resistivity.

To investigate the electronic contribution to the MIT, we measured the doping-dependent electronic structures using

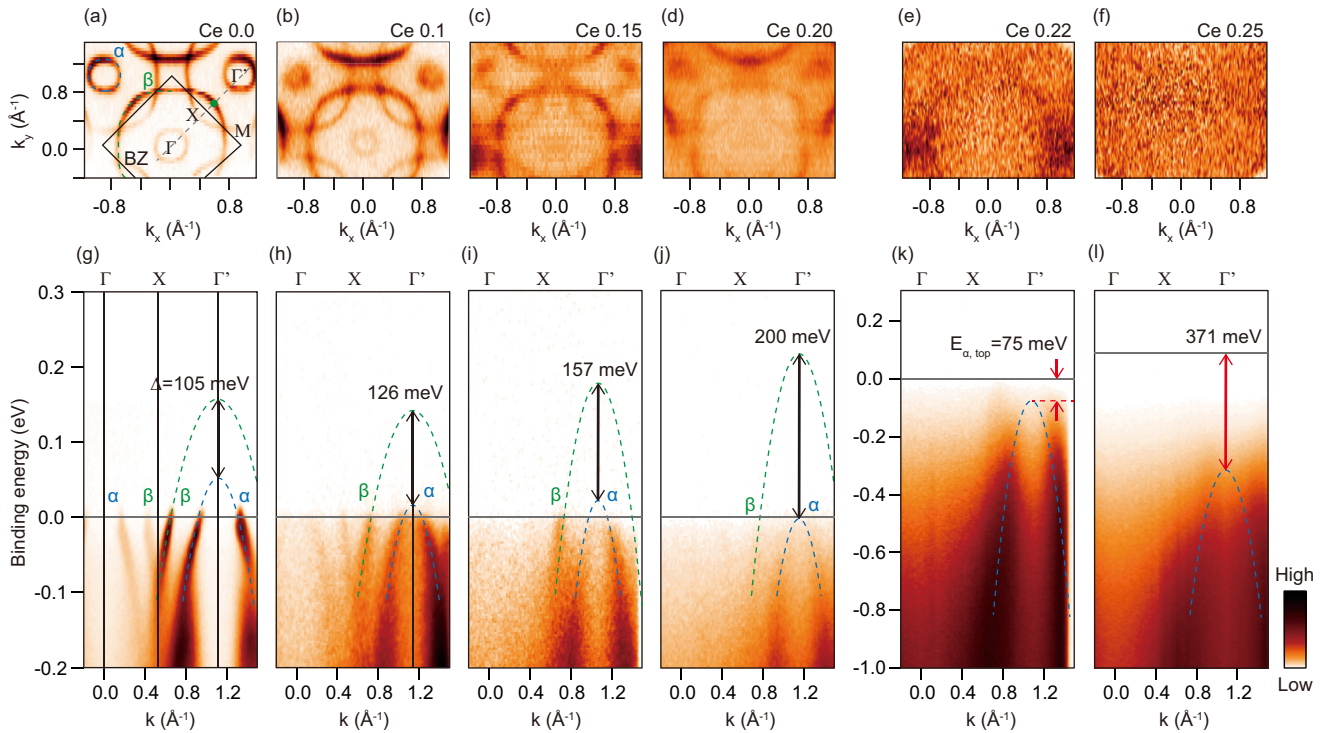


FIG. 2. Angle-resolved photoemission spectroscopy (ARPES) results using 70 eV photons. (a)–(f) Fermi-surface maps for various x values. The definitions of the bands, the Brillouin zone, and the high-symmetry points are given in (a). (g)–(l) Corresponding Ek data along the Γ -X, marked with a dashed line in (a). Parabolic fits of the experimental dispersions for the α (β) band are indicated by blue (green) dashed lines. The fitting method is described in the Supplemental Material (SM) [13]. The $E_{\alpha,\text{top}}$ indicates the α band top position, which is the ARPES visible gap.

ARPES as presented in Fig. 2. The Fermi surface of the end compound Sr_2RhO_4 consists of two bands: α and β bands [25–27]. As marked in Figs. 2(a) and 2(g), the α band is a small hole band around the Γ point, while the β band is an electron band that crosses the Brillouin zone boundary. As electrons provided from the Ce substitution are doped into the system, the bands show a rigid band shift as the parabolic fittings in Figs. 2(g)–2(i) show. However, no change is observed in the Fermi-surface topology of the two bands in the Ce concentration range of $0 \leq x \leq 0.15$ [Figs. 2(a)–2(c)]. At the critical doping $x = 0.20$, the α band top ($E_{\alpha,\text{top}}$) locates just below the Fermi level and the β band spectral weight near the Fermi level almost disappears [Fig. 2(j)]. At $x \geq 0.22$ the α further sinks below the Fermi level, and the β band spectral weight vanishes completely, creating an insulating gap. Unlike the usual Mott gap, which collapses upon charge doping [28,29], the $E_{\alpha,\text{top}}$ gradually sinks beyond the critical doping, indicating that the ARPES gaps in Figs. 2(k) and 2(l) increase with further doping.

The overall physical properties and doping-dependent band evolution of SC are similar to those of SL [10]. Gaps are formed for the α and β bands upon electron doping. At the critical doping, the α band rigidly shifts down below the Fermi level, while the β band suddenly loses its spectral weight at the Fermi level. Although such similar behaviors of the SL and SC systems suggest an intimate connection between the two MIT mechanisms, it is important to find out at which doping the transitions in the two systems occur, in order to elucidate the connection.

The ARPES data analysis in Fig. 3 provides the doping-dependent evolution of SC and SL [10] electronic structures. Figure 3(a) is the doping-dependent $E_{\alpha,\text{top}}$. For both systems, the α band top initially moves slowly to the higher binding energy side upon doping, then it shifts abruptly after the critical doping (around $x = 0.2$ and 0.4 for Ce and La, respectively). A notable difference is the dopant-dependent critical doping, for which a full discussion will be given later. On the other hand, the β band shows the MIT in a different manner. The β band spectral weight at the Fermi level vanishes around the critical point, as shown in Fig. 3(b). However, unlike the α band case, the β does not show a rigid band shift. Instead, the spectral weight disappears at the Fermi level in the same fashion as a Mott-Hubbard transition case [30,31].

To track the evolution of the band in the energy axis, Fig. 3(c) plots the momentum-averaged energy distribution curves from the β band Fermi surface in the first Brillouin zone. The β band quasiparticle stays at the Fermi level during the metallic regime ($0 \leq x \leq 0.2$) but is gradually suppressed. Meanwhile, the α and γ (fully occupied t_{2g}) bands are located below the Fermi level (blue shaded area). As the β peak disappears, the spectral weight below the Fermi level (blue and green shaded areas) appears to increase, which can be interpreted as the spectral weight transfer from the coherent β band. Such a gap formation as well as spectral weight transfer are consistent with the known behavior upon Mott-like correlation gap formation in the β band [30,31].

As the study on the SL suggested that the full occupation of the α ($J_{\text{eff}} = 3/2$) band triggers the β ($J_{\text{eff}} = 1/2$) band

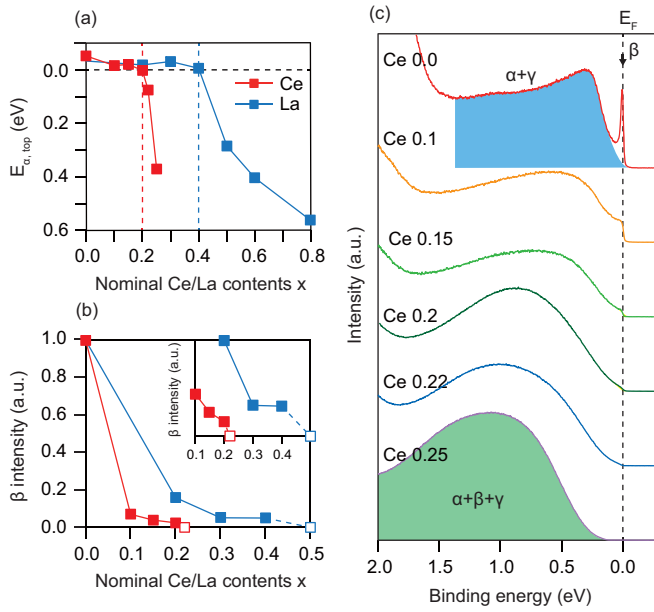


FIG. 3. Analysis results of the SC and $\text{Sr}_{2-x}\text{La}_x\text{RhO}_4$ (SL) ARPES data. The SL ARPES data were acquired at ALS Beamline 4.0.3 [10]. (a) Doping-dependent $E_{\alpha, \text{top}}$ estimated using the parabolic fits in Figs. 2(g)–2(l). Critical doping determined from the resistivity and ARPES data of SC (SL) is indicated by the red (blue) vertical dashed line. (b) Doping-dependent β band spectral weights. The spectral weight is obtained from the Fermi level momentum distribution curves (MDCs) extracted along the Γ - Γ' direction. The β band used for the analysis is indicated by the green point in Fig. 2(a). Please see the SM for details. The inset is a magnified image without the nondoped sample. (c) The β band energy distribution curves (EDCs) averaged along the Fermi momenta of the β band in the first Brillouin zone. Blue indicates the α and γ contributions, whereas green indicates the α , β , and γ contributions.

suppression [10], we propose that SC also has the same MIT mechanism. This can be expanded to an argument that any charge doping in Sr_2RhO_4 which can push the α band below the Fermi level will lead to the same mechanism of gap opening.

An important question is what is the difference between the SC and SL. Figure 4 shows results of a further analysis of the ARPES data with the help of the tight-binding (TB) calculations. Figure 4(a) shows the changes in the electron numbers, Δn_e , as a function of the nominal doping values x of La and Ce. It is seen that the La substitution has almost a linear relationship with Δn_e . On the other hand, Ce has one more electron than La. However, the actual estimation of Δn_e is less than two electrons per atom, which may be due to disorder driven localization or a partial formation of the localized f electrons [32]. As a result, at the critical doping ($x = 0.2$ for Ce and $x = 0.4$ for La), Δn_e is approximately $0.287e$ for the Ce and $0.365e$ for the La. Thus, the SC requires fewer electrons to fully occupy the α band to trigger the MIT, which may be due to a dopant-dependent band renormalization. An easy to imagine culprit for the different band renormalization may be the difference in the lattice constant change due to a dopant-induced chemical pressure. Figure 4(b) compares the a - and c -axis lattice constants as a function of Δn_e for

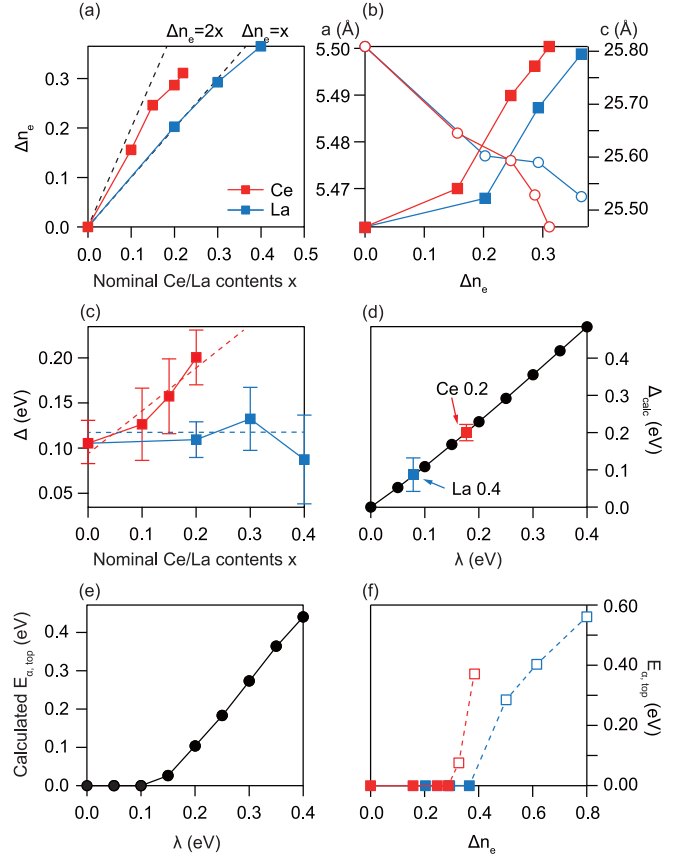


FIG. 4. Doping-dependent properties of SC and SL. (a) Total electron number determined from the ARPES data in the SM using the Luttinger theorem [13]. (b) a - and c -axis lattice parameters estimated from the XRD data in Fig. 1(a) (detailed fitting is given in the SM [13]). (c) Band splitting (Δ) between the α and β bands at the Γ point obtained via parabolic fittings in Figs. 2(g)–2(l) (described in the SM [13]). (d) Calculated Δ as a function of the SOC strength, λ , obtained by tight-binding (TB) calculations. Overlays are measured Δ values for Ce $x = 0.2$ and La $x = 0.4$. Using the calculated Δ line, we can obtain the effective SOC values for the two systems. (e) Calculated $E_{\alpha, \text{top}}$ as a function of λ from TB calculations. (f) $E_{\alpha, \text{top}}$ extracted from integrated EDCs of SC and SL [as defined in Figs. 2(k) and 2(l)] depending on the total electron numbers estimated from (a). Total electron numbers of insulating compounds (open squares) are estimated by extrapolation of (a).

the two systems. It is seen that the lattice constants gradually vary upon electron doping for both dopants. At the critical points, the lattice constants of the $\text{Sr}_{1.8}\text{Ce}_{0.2}\text{RhO}_4$ ($a = 5.4962$ Å, $c = 25.528$ Å) and $\text{Sr}_{1.6}\text{La}_{0.4}\text{RhO}_4$ ($a = 5.4988$ Å, $c = 25.526$ Å) have a less than 0.05% difference, which is unlikely to significantly alter the electronic structures [33,34].

Instead, we attribute the difference in the critical electron doping to the enhancement of the band hybridization near the Fermi level, which is often referred to as effective SOC in previous studies [8,35–37]. Plotted in Fig. 4(c) is Δ , the band splitting between the α and β bands at Γ , for the two systems. The Δ shows a significant dopant-dependent evolution. While the Δ has a relatively small x dependence for the La-doped case, far more change (about 95 meV) is observed for the Ce-doped case. Previous studies have shown that Δ is

proportional to the SOC [8]. Therefore, the increase in Δ may be interpreted as an increase in the effective SOC strength (λ_{eff}). Figure 4(d) shows a linear relationship between the TB calculated SOC strength λ and Δ values. Based on Fig. 4(d) and estimated Δ values in SM [13], we find that the effective SOC strength for SC ($x = 0.2$) and SL ($x = 0.4$) are 177 and 79 meV, respectively (106 meV for undoped Sr_2RhO_4). The Δ analysis and the TB calculations reveal that the effective SOC in the two systems can be significantly different. This difference in the effective SOC may lead to the difference in the critical electron doping of the two systems.

Here, we discuss how the effective SOC is related to the critical electron doping, for which we focus on SOC driven band reconstruction of the α and β bands. Since the α and β bands are from nearly J_{eff} states, a larger SOC may increase the J_{eff} projection and will split the two bands further, i.e., the α band of SC ($x = 0.2$) is lowered compared to that of SL ($x = 0.4$). As a result, SC requires less electron doping to push the α band below the Fermi level, and thus has a smaller critical electron number to have MIT compared to SL as seen in Fig. 4(f). The TB calculations support this idea as presented in Fig. 4(e) where the calculated $E_{\alpha, \text{top}}$ as a function of SOC is shown. A sufficiently large SOC can sink the α band below the Fermi level. The validity of this interpretation can be also seen in the doping-dependent, measured $E_{\alpha, \text{top}}$ in Fig. 4(f). SC shows a much stiffer enhancement of the $E_{\alpha, \text{top}}$ by the increasing electron number compared to SL. This is due to the larger SOC strength of the Ce-substituted system and corresponding strong band renormalization.

Based on the parameters extracted from the data, the MIT phase diagram as a function of the effective SOC and electron number is constructed as depicted in Fig. 5. The metallic phase exists where both the α and β bands cross the Fermi level. When the effective SOC is small, the two bands are not split enough that electron doping may not sink the α band below the Fermi level. Thus, both the α and β bands remain metallic. A strong effective SOC ($\lambda_{\text{eff}} \geq 0.4$ eV) such as the one in Sr_2IrO_4 almost fully splits the α and β bands [1,38]. As a result, the α band is located below the Fermi level, even without electron doping. In that case, the system may form a single $J_{\text{eff}} = 1/2$ band Mott phase with a half-filled β band. At an intermediate effective SOC, the interplay between the effective SOC and the electron number may determine the $E_{\alpha, \text{top}}$ as we discussed for the SC and SL systems. The gap becomes larger when the electron doping or the effective SOC push the $E_{\alpha, \text{top}}$ further below from the Fermi level. Therefore, a domelike metallic phase is formed, surrounded by the insulating phase. The phase diagram implies that we can vary the

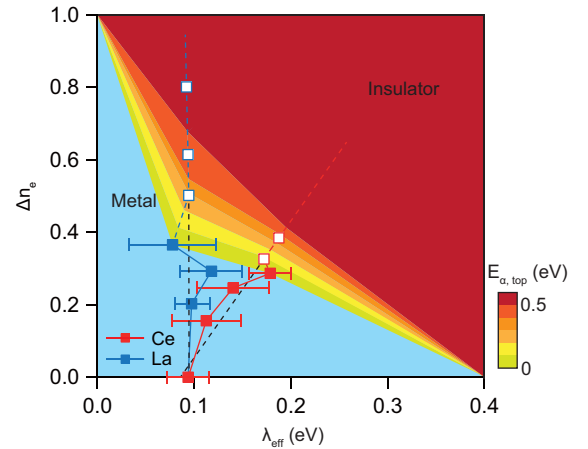


FIG. 5. Phase diagram of electron-doped Sr_2RhO_4 . The phase boundary between the metallic and insulating phases is taken as the midway between the metallic (solid squares) and insulating (open squares) phases. The actual electron numbers of the insulating phases are estimated via linear extrapolation of the data in Fig. 4(a). The color scale in the insulating phase represents the $E_{\alpha, \text{top}}$ shown by the scale bar.

electron doping and effective SOC to control the gap of the system.

Our findings may be expanded to various systems with multiband structures near the Fermi level. Here, the SOC driven band split is a key ingredient of the band structure to have the MIT. However, we point out that any system with multibands near the Fermi level with a proper degeneracy lifting mechanism can have a doping-dependent MIT. As $4d$ TMOs possess d bands near the Fermi level [24,39], other $4d$ TMOs may be good candidates to find new doping-dependent MITs.

This work was supported by the Institute for Basic Science in Korea (Grant No. IBS-R009-G2) and also by the National Research Foundation of Korea (NRF) grant funded by the Korea government (MSIT) (No. 2022R1A3B1077234). Research conducted at MAX IV, a Swedish national user facility, is supported by the Swedish Research Council under Contract No. 2018-07152, the Swedish Governmental Agency for Innovation Systems under Contract No. 2018-04969, and Formas under Contract No. 2019-02496. The Advanced Light Source is supported by the Office of Basic Energy Sciences of the U.S. DOE under Contract No. DE-AC02-05CH11231.

- [1] B. J. Kim, H. Jin, S. J. Moon, J.-Y. Kim, B.-G. Park, C. S. Leem, J. Yu, T. W. Noh, C. Kim, S.-J. Oh, J.-H. Park, V. Durairaj, G. Cao, and E. Rotenberg, *Phys. Rev. Lett.* **101**, 076402 (2008).
- [2] X. Wan, A. M. Turner, A. Vishwanath, and S. Y. Savrasov, *Phys. Rev. B* **83**, 205101 (2011).
- [3] K.-Y. Yang, Y.-M. Lu, and Y. Ran, *Phys. Rev. B* **84**, 075129 (2011).
- [4] J. Chaloupka, G. Jackeli, and G. Khaliullin, *Phys. Rev. Lett.* **105**, 027204 (2010).

- [5] Y. Singh, S. Manni, J. Reuther, T. Berlijn, R. Thomale, W. Ku, S. Trebst, and P. Gegenwart, *Phys. Rev. Lett.* **108**, 127203 (2012).
- [6] J. Yamaura, K. Ohgushi, H. Ohsumi, T. Hasegawa, I. Yamauchi, K. Sugimoto, S. Takeshita, A. Tokuda, M. Takata, M. Udagawa, M. Takigawa, H. Harima, T. Arima, and Z. Hiroi, *Phys. Rev. Lett.* **108**, 247205 (2012).
- [7] M. W. Haverkort, I. S. Elfimov, L. H. Tjeng, G. A. Sawatzky, and A. Damascelli, *Phys. Rev. Lett.* **101**, 026406 (2008).

- [8] J. Kwon, B. S. Kim, M. K. Kim, J. Denlinger, A. Bostwick, E. Rotenberg, N. Lee, H. Y. Choi, J. Y. Moon, Y. J. Choi, J. Mun, M. Kim, Y. Yoshida, W. Kyung, and C. Kim, *Phys. Rev. B* **103**, L081104 (2021).
- [9] K. W. Plumb, J. P. Clancy, L. J. Sandilands, V. V. Shankar, Y. F. Hu, K. S. Burch, H.-Y. Kee, and Y.-J. Kim, *Phys. Rev. B* **90**, 041112(R) (2014).
- [10] J. Kwon, M. Kim, D. Song, Y. Yoshida, J. Denlinger, W. Kyung, and C. Kim, *Phys. Rev. Lett.* **123**, 106401 (2019).
- [11] C. Martins, M. Aichhorn, L. Vaugier, and S. Biermann, *Phys. Rev. Lett.* **107**, 266404 (2011).
- [12] I. Nagai, N. Shirakawa, N. Umeyama, and S.-I. Ikeda, *J. Phys. Soc. Jpn.* **79**, 114719 (2010).
- [13] See Supplemental Material at <http://link.aps.org/supplemental/10.1103/PhysRevB.106.L241114> for the energy dispersive x-ray spectroscopy analysis, the details of ARPES data analysis, the XRD analysis, and the TB calculation procedure.
- [14] A. G. Zabrodskii, A. G. Andreev, and S. V. Egorov, *Phys. Stat. Sol. B* **205**, 61 (1998).
- [15] A. G. Zabrodskii, *Philos. Mag. B* **81**, 1131 (2001).
- [16] A. L. Efros and B. I. Shklovskii, *J. Phys. C* **8**, L49 (1975).
- [17] N. F. Mott, *Philos. Mag.* **26**, 1015 (1972).
- [18] I. Hase and Y. Nishihara, *J. Phys. Soc. Jpn.* **65**, 3957 (1996).
- [19] M. Itoh, T. Shimura, Y. Inaguma, and Y. Morii, *J. Solid State Chem.* **118**, 206 (1995).
- [20] R. D. Shannon, *Acta Cryst. A* **32**, 751 (1976).
- [21] O. Friedt, M. Braden, G. Andr e, P. Adelman, S. Nakatsuji, and Y. Maeno, *Phys. Rev. B* **63**, 174432 (2001).
- [22] V. I. Anisimov, I. A. Nekrasov, D. E. Kondakov, T. M. Rice, and M. Sigrist, *Eur. Phys. J. B* **25**, 191 (2002).
- [23] J. P. Carlo, T. Goko, I. M. Gat-Malureanu, P. L. Russo, A. T. Savici, A. A. Aczel, G. J. MacDougall, J. A. Rodriguez, T. J. Williams, G. M. Luke, C. R. Wiebe, Y. Yoshida, S. Nakatsuji, Y. Maeno, T. Taniguchi, and Y. J. Uemura, *Nat. Mater.* **11**, 323 (2012).
- [24] M. Kim, J. Kwon, C. H. Kim, Y. Kim, D. Chung, H. Ryu, J. Jung, B. S. Kim, D. Song, J. D. Denlinger, M. Han, Y. Yoshida, T. Mizokawa, W. Kyung, and C. Kim, *npj Quantum Mater.* **7**, 59 (2022).
- [25] R. S. Perry, F. Baumberger, L. Balicas, N. Kikugawa, N. J. C. Ingle, A. Rost, J. F. Mercure, Y. Maeno, Z. X. Shen, and A. P. Mackenzie, *New J. Phys.* **8**, 175 (2006).
- [26] F. Baumberger, N. J. C. Ingle, W. Meevasana, K. M. Shen, D. H. Lu, R. S. Perry, A. P. Mackenzie, Z. Hussain, D. J. Singh, and Z.-X. Shen, *Phys. Rev. Lett.* **96**, 246402 (2006).
- [27] I. Battisti, W. O. Tromp, S. Ricco, R. S. Perry, A. P. Mackenzie, A. Tamai, F. Baumberger, and M. P. Allan, *npj Quantum Mater.* **5**, 91 (2020).
- [28] Y. Cao, Q. Wang, J. A. Waugh, T. J. Reber, H. Li, X. Zhou, S. Parham, S.-R. Park, N. C. Plumb, E. Rotenberg, A. Bostwick, J. D. Denlinger, T. Qi, M. A. Hermele, G. Cao, and D. S. Dessau, *Nat. Commun.* **7**, 11367 (2016).
- [29] A. de la Torre, S. McKeown Walker, F. Y. Bruno, S. Ricc o, Z. Wang, I. Gutierrez Lezama, G. Scheerer, G. Girit, D. Jaccard, C. Berthod, T. K. Kim, M. Hoesch, E. C. Hunter, R. S. Perry, A. Tamai, and F. Baumberger, *Phys. Rev. Lett.* **115**, 176402 (2015).
- [30] Y. Wang, Y. He, K. Wohlfeld, M. Hashimoto, E. W. Huang, D. Lu, S.-K. Mo, S. Komiya, C. Jia, B. Moritz, Z.-X. Shen, and T. P. Devereaux, *Commun. Phys.* **3**, 210 (2020).
- [31] M. Sing, S. Glawion, M. Schlachter, M. R. Scholz, K. Go , J. Heidler, G. Berner, and R. Claessen, *Phys. Rev. Lett.* **106**, 056403 (2011).
- [32] G. A. Cabrera-Pasca, B. Bosch-Santos, A. Burimova, E. L. Correa, and A. W. Carbonari, *AIP Adv.* **10**, 015223 (2020).
- [33] M. Moreau, A. Marthinsen, S. M. Selbach, and T. Tybell, *Phys. Rev. B* **95**, 064109 (2017).
- [34] J.-H. Park, S. H. Lee, C. H. Kim, H. Jin, and B.-J. Yang, *Phys. Rev. B* **99**, 195107 (2019).
- [35] G.-Q. Liu, V. N. Antonov, O. Jepsen, and O. K. Andersen, *Phys. Rev. Lett.* **101**, 026408 (2008).
- [36] A. Tamai, M. Zing, E. Rozbicki, E. Cappelli, S. Ricc o, A. de la Torre, S. McKeown Walker, F. Y. Bruno, P. D. C. King, W. Meevasana, M. Shi, M. Radovi c, N. C. Plumb, A. S. Gibbs, A. P. Mackenzie, C. Berthod, H. U. R. Strand, M. Kim, A. Georges, and F. Baumberger, *Phys. Rev. X* **9**, 021048 (2019).
- [37] B. Zwartsenberg, R. P. Day, E. Razzoli, M. Michiardi, N. Xu, M. Shi, J. D. Denlinger, G. Cao, S. Lder, K. Ueda, J. Bertinshaw, H. Takagi, B. J. Kim, I. S. Elfimov, and A. Damascelli, *Nat. Phys.* **16**, 290 (2020).
- [38] J. Kim, D. Casa, M. H. Upton, T. Gog, Y.-J. Kim, J. F. Mitchell, M. van Veenendaal, M. Daghofer, J. van den Brink, G. Khaliullin, and B. J. Kim, *Phys. Rev. Lett.* **108**, 177003 (2012).
- [39] A. Georges, L. de' Medici, and J. Mravlje, *Annu. Rev. Condens. Matter Phys.* **4**, 137 (2013).